

Universal Model for 3D Medical Image Analysis

Xiaoman Zhang, Ya Zhang, Xiaoyun Zhang, and Yanfeng Wang

Abstract—Deep Learning-based methods recently have achieved remarkable progress in medical image analysis, but heavily rely on massive amounts of labeled training data. Transfer learning from pre-trained models has been proposed as a standard pipeline on medical image analysis to address this bottleneck. Despite their success, the existing pre-trained models are mostly not tuned for multi-modal multi-task generalization in medical domains. Specifically, their training data are either from non-medical domain or in single modality, failing to attend to the problem of performance degradation with cross-modal transfer. Furthermore, there is no effort to explicitly extract multi-level features required by a variety of downstream tasks. To overcome these limitations, we propose Universal Model, a transferable and generalizable pre-trained model for 3D medical image analysis. A unified self-supervised learning scheme is leveraged to learn representations from multiple unlabeled source datasets with different modalities and distinctive scan regions. A modality invariant adversarial learning module is further introduced to improve the cross-modal generalization. To fit a wide range of tasks, a simple yet effective scale classifier is incorporated to capture multi-level visual representations. To validate the effectiveness of the Universal Model, we perform extensive experimental analysis on five target tasks, covering multiple imaging modalities, distinctive scan regions, and different analysis tasks. Compared with both public 3D pre-trained models and newly investigated 3D self-supervised learning methods, Universal Model demonstrates superior generalizability, manifested by its higher performance, stronger robustness and faster convergence. The pre-trained Universal Model is available at: <https://github.com/xm-cmic/Universal-Model>.

Index Terms—Transfer learning, multi-modality, adversarial learning, pre-trained model, 3D medical image

I. INTRODUCTION

DEEP learning-based models have recently made remarkable progress in various computer vision tasks, such as object detection and semantic segmentation. However, the success of these data-driven approaches generally demands massive amounts of annotated training data [1]. To reduce the requirement on training data size, a simple transfer learning scheme, i.e. pre-training the model with a large-scale dataset such as ImageNet [2] and then fine-tuning it with training data specific to the target task, has been widely adopted. Previous studies [1], [3] indicate that knowledge transfer from large-scale well-annotated natural images to medical images is valuable on the Computer-Aided Diagnosis (CAD) problems. However, limited by the fact that typical medical imaging

modalities such as computed tomography (CT), magnetic resonance imaging (MRI), and positron emission tomography (PET) are 3D volumes, ImageNet pre-trained model cannot be directly applied to the medical images. The common exemplar is converted 3D volume data into 2D slices, disregarding rich 3D spatial anatomical information, thereby inevitably compromising the performance. Considering this problem, some other studies [4], [5] transfer from the 3D public available models pre-trained on the natural video recognition dataset [6], [7], but have not yielded the desired results due to the comparatively large differences between video and 3D medical data.

A pre-trained 3D model is important for the development of deep learning models for medical image analysis. Unfortunately, obtaining a comprehensively annotated dataset like ImageNet in medical domain is extremely challenging, if not prohibitive. Not only does medical image annotation requires a lot of labor and time costs, but also requires expert annotation by trained physicians, who are difficult to be recruited in large scale. Moreover, in real-world practice, it is usually impossible to collect extensive samples from a single clinical center. Data from different centers, however, present apparent heterogeneity. The discrepancies inherent in multi-center data raise cross-domain challenges when combining samples from different centers for model training [8].

In addition to pre-training on high-quality annotated data [9], a feasible alternative is to leverage self-supervised learning [10]–[13] in pre-training. A generic framework is to first employ predefined proxy tasks to learn feature representations capturing the data characteristics via self-supervision, and further fine-tune the target model with a handful of task-specific annotated data. Despite their promises in 3D medical image analysis, the above methods come with two limitations. First, existing models are mostly developed for a specific modality and do not address the cross-modality generalization issues. Medical images come in multiple related modalities, e.g. CT and MRI, each with distinct image appearance reflecting responses to different anatomical structures of the body. Training a single pre-trained generalizable model covering different modalities is a desired but non-trivial task [8]. Second, previous studies that leverage multiple data sets to build a pre-trained model, usually ignored the domain gap between them. However, data collected with different imaging equipment and scanning protocols could be quite different in factors such as spatial resolution and slice thickness. It is necessary to attend such domain gap in learning with multi-center data.

In this paper, we aim to exploit the publicly available datasets to build a generalizable pre-trained model that can be effectively adopted by a variety of 3D medical image analysis tasks in multiple modalities. We propose to train the

X. Zhang, Y. Zhang, X. Zhang, Y. Wang are with the Cooperative Medianet Innovation Center, Shanghai Jiao Tong University. (Email: {xm99sjtu, ya_zhang, xiaoyun.zhang, wangyanfeng}@sjtu.edu.cn)

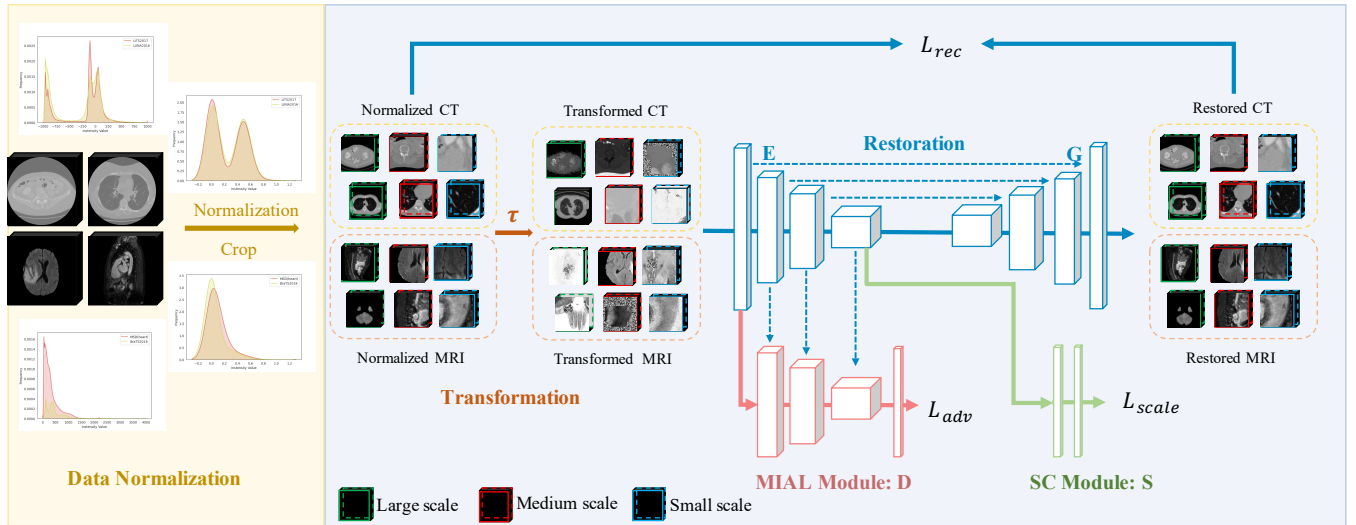


Fig. 1. Schematic diagram of the proposed method. Universal Model is then trained based on a basic self-supervised learning (SSL) framework, which learns representations by reconstructing the original sub-volumes after a certain transformation τ . The MIAL module D is used to enforce the cross-modality transferability of the features through adversarial learning and the SC module S is introduced to enhance the generalizability to multiple tasks by learning multi-level features. To account for distribution discrepancy between data set, the input data were pre-processed with spatial and intensity normalization.

Universal Model, a generic pre-trained model for 3D medical imaging, based on a self-supervised learning (SSL) framework that learns representations from unlabeled data. Fig. 1 shows the overall framework of the Universal Model training. All the input data are first processed with spatial and intensity normalization to mitigate the heterogeneity among multi-center datasets, and then cropped to sub-volumes of different scales as inputs. Following [14], we take image restoration as the self-supervised learning task, recovering original sub-volumes from various transformations. To tackle the cross-modality generalization issue, we design a modality invariant adversarial learning (MIAL) module to learn general feature representations. With regards to the generalization to multiple tasks, as different medical image analysis tasks may rely on different levels of semantic features, e.g., Alzheimer classification tends to utilize low-level local features corresponding to the detailed texture information while organ segmentation requires high-level global features, multi-level features are essential for effective generalization to a wide range of target tasks. To make the model generalizable to a variety of tasks, a scale classifier (SC) module is further introduced to recognize the scales of the input sub-volumes and thereby help capture features at different levels.

We validate the effectiveness and the generalization capability of our proposed model from multiple perspectives. Extensive experiments on five different target tasks have demonstrated that the pre-trained model can consistently improve the performance on all tasks and outperform the state-of-the-art approaches. To the best of our knowledge, this is the first work investigating 3D pre-trained model that leverages multi-modal multi-center datasets to enable better transferability towards various medical images analysis tasks. The main contributions of this paper are summarized as follows:

- **Modality Invariant Representation Learning:** We design a modality invariant adversarial learning module to guide

the pre-trained model to capture more robust and generalizable representations from multi-modality data.

- **Multi-level Feature Learning:** We propose a scale classifier to distinguish the input scale, which can make the network capture discriminative visual descriptions at different levels and further improve the transfer performance on a wide range of tasks.

II. RELATED WORK

A. Transfer Learning for Medical Image Analysis

To improve the performance with limited annotated data and accelerate the convergence speed, a variety of transfer learning methods have been applied in medical image analysis [15]–[18]. Transfer learning from large-scale natural image datasets, initializing models with corresponding pre-trained weights has become the predominant method for deep learning applications to medical imaging. For example, Esteva *et al.* [19] solved the skin lesion classification task using Google Inception v3 CNN architecture [20] pre-trained on the ImageNet dataset. Tajbakhsh *et al.* [21] initialized the deep architectures with pre-trained models to embed knowledge transferred from the ImageNet for pulmonary embolism diagnosis. Although these methods have proved to be beneficial for improving the performance of medical image tasks, there remains a large domain gap between the natural video data and medical image. Meanwhile, such supervised representation learning methods rely heavily on well-labeled data while generating annotations of medical images is invariably expensive and time-consuming.

Recently, some works utilized self-supervised learning methods to address this limitation, encouraging the network to learn image representation from unlabeled data. Taleb *et al.* [22] integrated multi-modal MRI medical imaging datasets, and designed puzzle-solving with varying levels of puzzle

complexity as a pretest task, facilitating the learning of downstream tasks. Zhuang *et al.* [12] proposed a novel proxy task, i.e. Rubik's cube recovery, for the volumetric medical images. Chen *et al.* [11] combined image rotation with local shuffling as the surrogate task, where the model is trained to restore the altered image to its original version. Taleb *et al.* [23] presented 3D versions for five self-supervised learning methods and demonstrated the effectiveness for medical image application. These works, however, are developed individually for specific downstream tasks. Zhou *et al.* [10] first proposed Model Genesis, a pre-trained 3D model by learning from a self-supervised framework on a chest CT dataset, which demonstrated the effectiveness and necessity of the 3D medical pre-training model. Haghighi *et al.* [24] further proposed to extend the self-supervised framework with self-discovery and self-restoration to learn semantically enriched features. One main limitation of the aforementioned methods is that only a single modality dataset is used for model pre-training, ignoring the significant differences in distribution and appearance between different modalities, while our work aims to leverage multi-modality datasets to improve the performance on different modalities simultaneously.

B. Domain Invariant Adversarial Learning

Prior adversarial learning methods [25]–[28] have shown impressive results in domain adaptation tasks, transferring knowledge from the source domain to the target domain. The basic algorithm is inspired by Generative Adversarial Network (GAN) [29], which exploits a generator to capture the data distribution of the training data and a discriminator to distinguish the real image and generated image. In domain adversarial learning, this principle has been employed to ensure that the learned representations are domain confused. For instance, Domain-adversarial Neural Network (DANN) [25] proposed a gradient reversal layer to ensure the similarity of feature distributions in the two domains. Li *et al.* [30] proposed to learn cross-domain invariant features using Maximum Mean Discrepancy (MMD) via adversarial feature learning.

Ideally, deep learning models deployed in medical imaging applications should be invariant to image appearance shifts caused by factors such as different imaging modalities, scanners or demographic properties. Recently, some related works are designed to mitigate domain gaps between different modalities. Dou *et al.* [31] conducted unsupervised domain adaptation with adversarial learning between CT and MRI for the cardiac segmentation task. Cheng *et al.* [32] introduced a new data-efficient method for cross-modality medical image segmentation by combining latent space learning with adversarial learning. In such situations, we employ the spirit of domain adaptation and domain generalization and explore how to incorporate the adversarial learning with the self-supervised learning scheme for better representation learning from different modalities data.

III. METHOD

A schematic of our approach is shown in Fig. 1. Universal Model is a generic pre-trained model for 3D medical imaging, leveraging multi-modal and multi-center data sets for

general representation learning, which can effectively transfer to various downstream medical imaging tasks. We preprocess the multi-center input data by spatial and intensity normalization to reduce the domain gap. Following [14], we adopt the 3D U-Net based image restoration proxy task as our baseline to learn robust representation. Based on the basic SSL framework, Universal Model consists of two modules to realize generalizable feature learning. First, we design a MIAL module, enabling the model to learn general feature representations by adversarial learning to tackle the cross-modality generalization issue. This is motivated by the fact that the target datasets have various modality and naively fusing multi-modal representations may lead to transfer performance degradation, thus the expected feature representation should be invariant to the modal information. Second, we devise a simple yet effective SC module, together with the multi-scale sub-volume input, to help capture features at different levels, so that our pre-trained model can be transferred to a variety of downstream tasks.

A. Self-supervised Framework

Self-supervised-based representation learning has been a new trend both in computer vision and medical image analysis [10]–[12]. Its central idea is to transfer general features extracted by the pretest task that can be trained without labeled data to the target tasks. Inspired by [14], we take the 3D U-Net [33] based image restoration proxy task as our backbone. Such architecture has two advantages. First, it can leverage a mixture of self-supervised tasks to learn diverse representations and show promising prospects for transfer learning [11], [34]. Second, it can be consolidated into a single 3D U-Net, which can be considered as the most commonly used backbone for 3D medical image analysis [35].

The goal of the self-supervised proxy task is to learn to recover origin sub-volumes x_i from transformed inputs \hat{x}_i , where $\hat{x}_i = \tau(x_i)$ and $\tau(\cdot)$ denotes the transformation function. In practice, we apply a sequence of image transformations to the input sub-volumes. We follow [14] and adopt the same set of transformations, i.e. non-linear, local-shuffling, inner and outer-painting, corresponding to the appearance, texture and context, respectively. The Mean Square Error (MSE) loss is employed as the optimization target for the restoration task and the optimizer function is expressed as:

$$\min_{\theta_E, \theta_G} L_{rec} = \sum_{x_i \in \mathcal{D}} \|G(E(\hat{x}_i)) - x_i\|_2, \quad (1)$$

where θ_E and θ_G are parameters of the encoder E and the decoder G , respectively.

B. Modality Invariant Adversarial Learning

Medical images in different modalities are quite different in characteristics. To avoid the performance degradation caused by cross-modality generalization, we develop a Modality Invariant Adversarial Learning (MIAL) module for modality invariant representation learning. Different from the common domain discriminator, which uses $E(\hat{x})$ as input, we contact features of different layers in E with the corresponding layer

in D , as shown in Fig. 1. Such a densely connected operation improves the modality invariant feature learning by strengthening the connection between the encoder and discriminator. If the discriminator can successfully classify the domain of input sub-volumes, it means that the extracted features still contain modality characteristics. Hence, we apply the minimax two-player game, where the discriminator D is trained to distinguish the domain label, and the encoder E is trained simultaneously to confuse the domain discriminator. Denote $\mathcal{D} = \{\mathcal{D}_{CT}, \mathcal{D}_{MRI}\}$ as the training dataset. The following adversarial loss is applied:

$$\min_{\theta_E} \max_{\theta_D} L_{adv} = \sum_{x_i^{CT} \in \mathcal{D}_{CT}} \log D(E(\hat{x}_i^{CT})) + \sum_{x_i^{MRI} \in \mathcal{D}_{MRI}} \log(1 - D(E(\hat{x}_i^{MRI}))), \quad (2)$$

where θ_E and θ_D are parameters of encoder E and discriminator D , x_i^{CT} and x_i^{MRI} are the resized input sub-volumes of corresponding modality.

C. Scale Classifier

To effectively exploit the multi-level contextual information, we design a SC module to distinguish the scale of inputs. In this way, Universal Model learns to utilize both representations at different levels, which is expected to improve the transfer performance on a variety of target tasks.

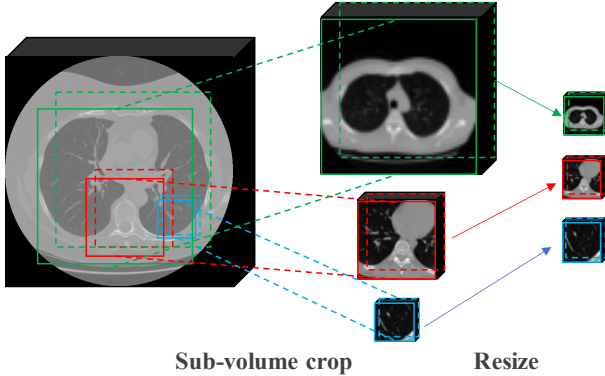


Fig. 2. Illustration of the multi-scale sub-volume extraction process. We first randomly crop sub-volumes at three different scales: large, medium and small, which correspond to the green, red, blue cubes in the figure. We then resized all the sub-volumes to the same size to fit the input size of the network.

For each volume in the training dataset \mathcal{D} , we first randomly crop sub-volumes of three different scales: large, medium and small, corresponding to approximately $1/2$, $1/4$ and $1/8$ of the side length of the original cube respectively. The numbers of large scale, medium scale and small scale are in the ratio $1 : 1 : 2$ as the small scale cubes can be more diverse. The exact number of cubes are shown in Table I. To fit the model input size, we then resize all the sub-volumes to the same size: $64 \times 64 \times 32$. Fig. 2 shows the pre-processing for input volumes. Let x_i denotes the resized input sub-volume and y_i is the corresponding scale label. We build a classifier S to classify the scale of input sub-volumes,

ensuring the learned representations containing multi-level of discriminative features. The optimizer function for SC module is defined as:

$$\min_{\theta_E, \theta_S} L_{scale} = \sum_{(x_i, y_i) \in \mathcal{D}} H(S(E(\hat{x}_i)), y_i), \quad (3)$$

where $H(\cdot)$ represents cross entropy loss, \hat{x}_i is the transformed input volumes, y_i is the corresponding scale labels, and θ_S are parameters of the scale classifier S .

D. Objective function

The final objective function for generating the pre-train model can thus be formulated as:

$$\min_{\theta_E, \theta_G, \theta_S} \max_{\theta_D} L_{adv} + \alpha L_{scale} + \beta L_{rec}, \quad (4)$$

where α and β are trade-off parameters weighting the loss functions, since the magnitudes of the three loss functions are inconsistent. In our experiments, we empirically set α and β as 1 and 10 respectively.

IV. EXPERIMENTS

A. Data Sets

The following six publicly available data sets, which cover two most popular medical image modalities and span a wide spectrum of tasks, are used to build and evaluate the pre-trained model. The model is first trained to learn image representation via proposed method on source datasets, and then fine-tuned with full supervision to yield a target model to solve specific problems (target tasks) in the same or different datasets (target datasets). Note that all the test images for target tasks are not exposed to model pre-training and fine-tuning stage for a fair comparison. Table II shows the usage of each dataset in the pre-training, fine-tuning, and test stage. If a data set is used for both the pre-training and fine-tuning stages, the two stages share the same train set. The difference is that the pre-training stage uses no annotations, but the fine-tuning stage does use the annotations.

1) **LUNA2016** [36]: The dataset contains 888 CT scans with slick thickness less than $2.5mm$ for nodule detection and false positive reduction. The annotations were collected during a two-phase annotation process using 4 experienced radiologists. CT scans are randomly assigned to a train set (623 cases) and a test set (265 cases) followed [14].

2) **LiTS2017** [37]: The dataset consists of 130 labeled CT scans for automatic segmentation of liver and tumor lesions. The dataset is collected from seven hospitals and research institutions and manually reviewed by three radiologists independently. CT scans are randomly assigned to a train set (111 cases) and a test set (19 cases), so that the trained model can be further tested on this data set.

3) **BraTS2018** [38], [39]: The dataset contains 285 volumes acquired with different MRI scanners, which consists of 210 high grade glioblastomas (HGG) and 75 low grade glioblastomas (LGG) cases. For each patient, a T1 weighted, a post-contrast T1-weighted, a T2-weighted and a Fluid-Attenuated Inversion Recovery (FLAIR) MRI were provided. Each tumor

TABLE I

STATISTICS OF THE PRE-TRAINING DATA SETS WHERE CASES REPRESENT VOLUMES USED IN THE PRE-TRAINED PROCESS AND SUB-VOLUME NUMBER REPRESENTS THE NUMBER OF CROPPED CUBES AT DIFFERENT SCALES.

Dataset	Cases	Modality	Organ	Median Shape	Median Spacing (<i>mm</i>)	Sub-volume number
LUNA2016	623	CT	Lung	$238 \times 512 \times 512$	(1.25, 0.74, 0.74)	(19936, 9968, 9968)
LiTS2017	111	CT	Liver	$432 \times 512 \times 512$	(1.00, 0.77, 0.77)	(7104, 3552, 3552)
BraTS2018	760	MRI(T1, T1c, T2, FLAIR)	Brain	$138 \times 169 \times 138$	(1.00, 1.00, 1.00)	(24320, 12160, 12160)
MSD (heart)	30	MRI	Heart	$115 \times 320 \times 232$	(1.37, 1.25, 1.25)	(1920, 960, 960)

TABLE II

THE DATA SETS USED FOR PRE-TRAINING, FINE-TUNING, AND TESTING OF THE UNIVERSAL MODEL. ✓ DENOTES WHETHER THE DATASET IS USED IN THE CORRESPONDING STAGE.

Dataset	Modality	Organ	Pre-training	Fine-tuning	Test
LUNA2016	CT	Lung	✓	✓	✓
LiTS2017	CT	Liver	✓		
BraTS2018	MRI	Brain	✓	✓	✓
MSD(heart)	MRI	Heart	✓		
MMWHS	MRI, CT	Heart		✓	✓
ADNI	MRI	Brain		✓	✓

was segmented into edema, necrosis and non-enhancing tumor and active/enhancing tumor. MRI volumes are randomly assigned to a train set (190 cases) and a test set (95 cases).

4) *MSD(heart)* [40]: The dataset contains 30 MRI datasets covering the entire heart acquired during a single cardiac phase. Each data was segmented into left atrium appendage, mitral plane, and portal vein endpoints by an expert using an automated tool followed by manual correction. Since the result submission website of this challenge is still accessed, all the MRI scans are used for model pre-training.

5) *MMWHS* [41], [42]: The dataset consists of unpaired 20 CT and 20 MRI images covering the whole heart substructures. Manual labeling for seven structures was adopted for generating the gold standard segmentation. We conduct experiments on CT and MRI respectively, and the data sets are randomly divided into a training set (16 cases) and a test set (4 cases).

6) *ADNI* [43]: The dataset contains 819 subjects covering multi-site MRI and PET data from AD patients, MCI patients, and elderly controls, each followed for 12 months using standard cognitive and functional measures typical of clinical trials. Specifically, we used data from the "spatially normalized, masked, and N3-corrected T1 MRI images" category following [44] for Alzheimer's Disease Classification, including 47 T1-weighted MRI scans from the Alzheimer's disease cohort (AD) and 56 MRI scans from the normal cohort (NC). MRI scans are randomly assigned to a train set (37 AD, 45 NC) and a test set (10 AD, 11 NC).

B. Pre-training Setup

1) *Data set and Normalization*: To validate the effectiveness of the proposed method, we employ the following four publicly available 3D medical image data sets, LUNA2016, LiTS2017, BraTS2018, and MSD (heart), as source data sets to build pre-trained models. The data sets are quite diverse, containing two modalities (i.e. MRI and CT) of data, from three different scan regions (i.e. brain, chest, and abdomen), and targeting on four organs (i.e. lung, liver, brain, and heart).

The detailed information about the source datasets is shown in Table I. The four data sets show very different data distribution as can be seen from Table I (spatial spacing) and Fig. 1 (intensity), due to the multi-modality, multi-center, and multi-task nature of the data. To alleviate the heterogeneity caused by multi-center (e.g. due to different scanners and imaging protocols), we process the data with spatial and intensity normalization. To cope with this spatial heterogeneity, we resample all volumes to the same voxel spacing ($1 \times 1 \times 1 \text{ mm}^3$) by using third-order spline interpolation. Meanwhile, for different medical imaging modalities, the range of intensity values vary significantly. To mitigate the side-effect of extreme pixel value, we clip the intensity values of CT volumes on the min (-1000) and max (+1000) interesting Hounsfield Unit range. And for the MRI volumes, all the intensity values are clipped on the min (0) and max (+4000) interesting range. Each volume is normalized independently to [0,1]. Fig. ?? shows the overall intensity histogram distributions of CT and MRI data sets before and after normalization. We can observe that after normalization, the intensity histogram distribution of the same modality is similar, while the distributions between CT and MRI are still divergent.

2) *Implementation*: The basic encoder E and decoder G follow the 3D U-Net [33] architecture with batch normalization. The MIAL module D is constructed with three convolution layers with a global average pooling (GAP) layer and two fully connected (FC) layers. Each convolution layer contains two $3 \times 3 \times 3$ convolution layers followed by a batch normalization layer, a ReLU layer and a $2 \times 2 \times 2$ max-pooling layer. The input of the D is the output of the first layer of encoder E . And the shortcut connections between E and D are the same as skip connections in U-Net architecture. The SC module S simply consists of a GAP layer and two FC layers, a layer with 1024 hidden units followed by final output. The network is trained using SGD optimizer, with an initial learning rate of $1e0, 1e-1, 1e-3$ for 3D U-Net, SC module (S), MIAL module (D) respectively. We use ReduceLROnPlateau to schedule the learning rate according to the validation loss. The model was implemented with a PyTorch framework on GTX 1080Ti GPU.

C. Fine-tuning Setup

1) *Target Tasks*: These target tasks are selected as diverse as possible in terms of organ, disease, modality, with varying levels of semantic distance from the source datasets used in pre-training, allowing us to investigate the transferability of the pre-trained Universal Model. We report test performance through the mean and standard deviation of five trials for each target task.

- **BTS (MRI):** We perform the brain tumor segmentation task using the train set of BraTS2018. Following the experiment strategy in [14], we use FLAIR images and only segment the whole brain tumor, and evaluate on the test set.
- **LNC (CT):** We perform the lung nodule false positive reduction task using the LUNA2016 dataset. 551,065 detection candidates of the lung nodules are provided with 1351 positive lung nodules as the train set. The test set contains 166225 candidates with 383 positive lung nodules.
- **LAS (CT):** We use the training set of CT data from the MMWHS dataset for left atrial blood cavity segmentation and evaluate on the test set.
- **LAS (MRI):** We use the training set of MRI data from the MMWHS dataset for left atrial blood cavity segmentation and evaluate on the test set.
- **ADC (MRI):** We perform the Alzheimer's Disease diagnosis task using the selected data from ADNI dataset followed the prior study [44] for Alzheimer's Disease Classification.

2) Implementation: Since our model is built on the commonly used 3D U-Net architecture, we transfer encoder-decoder for the target segmentation tasks with dice loss and transfer the encoder as the feature extraction backbone of the target classification tasks with cross-entropy loss. For segmentation tasks, we employ a commonly-used evaluation metric, the Intersection over Union (IoU) to evaluate the segmentation performance. For the false positive reduction task, we use the Area Under the Curve (AUC) score on classifying true positives and false positives to evaluate the performance. We optimize the network using the Adam optimizer [45] with a learning rate of $1e-3$ for fine-tuning, where $\beta_1 = 0.9$, $\beta_2 = 0.999$, $\epsilon = 1e-8$. Note that all of the layers in the model are trainable during fine-tuning. To improve the generalization ability, we augment the training sets of all target tasks by random flipping, transposing, rotating and Gaussian noise.

D. Comparison Methods and Implementation

To verify the effect of the proposed method, we compared our proposed pre-trained model with the state-of-the-art open-source 3D pre-trained models and the mainstream 3D self-supervised methods. The pre-trained models include: Inflated 3D (I3D) [6], NiftyNet [46], Med3D [9] and Model Genesis [14] and the self-supervised methods include: 3D Rotation and 3D Jigsaw [23]. Below we provide a brief summarization.

- **I3D [6]** is pre-trained on the video dataset Kinetics [47] targeted for action recognition. We duplicate the input sub-volume into two channels to align with the required input shape and expand a decoder with skip connections same as that implemented in our 3D U-Net for segmentation tasks.
- **NiftyNet [46]** is proposed as an open-source platform with a modular structure designed for sharing networks and pre-trained models using 90 abdominal CT cases in medical imaging analysis. Following the prior work, we use the Dense V-Networks [48] as the backbone for fine-tuning.
- **Med3D [9]** is a heterogeneous 3D network pre-trained on 3DSeg-8, a well-annotated dataset with diverse modalities and target organs. We use the pre-trained model with

ResNet-101 as the encoder, which reports the highest performance in the paper.

- **Model Genesis [14]** is a recently proposed pre-trained model for medical image based on a self-supervised framework. We use Genesis Chest CT (3D) for comparison, which is trained on LUNA2016 [36].
- **Taleb *et al.* [23]** extended existing self-supervised methods to 3D versions for medical imaging. 3D Jigsaw puzzle solving (3D Jigsaw) is to predict the permutation applied to the 3D volumes, where the puzzles are formed by shuffling the $3 \times 3 \times 3$ grid of 3D volumes according to the predefined permutations. 3D rotation prediction (3D Rotation) is to predict the angle of rotation applied to the input volumes. The permutation number and rotation degree setting follow the prior work. In practice, 3D Rotation and 3D Jigsaw are pre-trained by the proxy task on the fine-tuned dataset for each target task.

The experiments on these compared methods are conducted by using the released codes and pre-trained models. To ensure a fair comparison, we re-run the codes on the five target datasets employed in this work with the same pre-processing steps and model settings. Note that all methods use the same data in fine-tuning and testing stage.

V. RESULTS

A. Comparison With State-of-the-Art Methods

In this section, we first compare Universal Model with training from scratch and then conduct comparison with the state-of-the-art methods. The overall results in terms of four target tasks are summarized in Table III. Note that the results on the BraTS2018 and LUNA2016 datasets of the state-of-the-art methods are directly reported from original paper [14].

Compared with training from scratch, fine-tuning on a pre-trained model generally yields better results, but not consistently for all tasks. We can see that I3D leads to 9.31%, 8.34% improvements of IoU score on the BTS (MRI) and LAS (CT) task, but does not perform well on LAS (MRI). We attribute this to the fact that transfer learning boosts performance only when the representation learned from the pre-trained model is favorable to the target tasks. This verifies the necessity of a generic pre-trained model for multi-modality 3D medical image tasks. Compared with existing pre-trained models or self-supervised approaches, the proposed Universal Model leads to consistently better results on all target tasks. For example, Universal Model outperforms Model Genesis with 4.14%, 0.70%, 1.66%, 2.99%, 7.11% improvements of the evaluation metrics on BTS (MRI), LNC (CT), LAS (CT), LAS (MRI) and ADC (MRI), respectively. Note that, even for the lung node false positive reduction task which is used in pre-training, we also gain improvements. It implies that our model can obtain a more robust and generalizable representation. Fig. 3 shows the representative examples of the segmentation tasks produced by the compared methods on the test dataset. It is observed that Universal Model achieves much better results, while the other methods may segment the irrelevant area framed by the orange boxes.

TABLE III

COMPARISON OF UNIVERSAL MODEL AND STATE-OF-THE-ART APPROACHES. NOTE WHILE THE METHODS MAY USE DIFFERENT DATA SETS FOR PRE-TRAINING, ALL METHODS ARE FINE-TUNED AND TESTED WITH THE SAME SET OF DATA. THE FIRST ROW SHOWS WHETHER THE FINE-TUNING SET OF THE TARGET TASK IS USED FOR UNIVERSAL MODEL PRE-TRAINING.

Pre-training	Approach	Used to Pre-train Universal Model		Not Used to Pre-train Universal Model		
		BTS (MRI) IoU (%)	LNC(CT) AUC (%)	LAS (CT) IoU (%)	LAS (MRI) IoU (%)	ADC (MRI) AUC (%)
No	Train from scratch	58.52 ± 2.61	94.25 ± 5.07	68.29 ± 1.68	67.04 ± 2.18	74.00 ± 3.82
Supervised	I3D [6]	67.83 ± 0.75	98.26 ± 0.27	76.63 ± 2.32	66.71 ± 1.27	74.44 ± 2.53
	NiftyNet [46]	60.78 ± 1.60	94.14 ± 4.57	74.91 ± 2.78	64.60 ± 1.96	73.21 ± 3.18
	Med3D [9]	66.09 ± 1.35	95.80 ± 0.49	75.01 ± 0.74	63.43 ± 0.61	82.00 ± 3.01
Self-Supervised	3D Rotation [23]	56.48 ± 1.78	97.13 ± 0.81	67.54 ± 2.80	71.36 ± 1.70	78.44 ± 4.59
	3D Jigsaw [23]	59.65 ± 0.81	96.12 ± 0.63	68.40 ± 2.92	72.99 ± 2.54	76.44 ± 1.47
	Model Genesis [14]	67.96 ± 1.29	98.34 ± 0.44	76.48 ± 2.89	74.53 ± 1.69	79.33 ± 2.29
	Universal Model (Ours)	72.10 ± 0.67	99.04 ± 0.23	78.14 ± 0.77	77.52 ± 0.50	86.44 ± 1.09

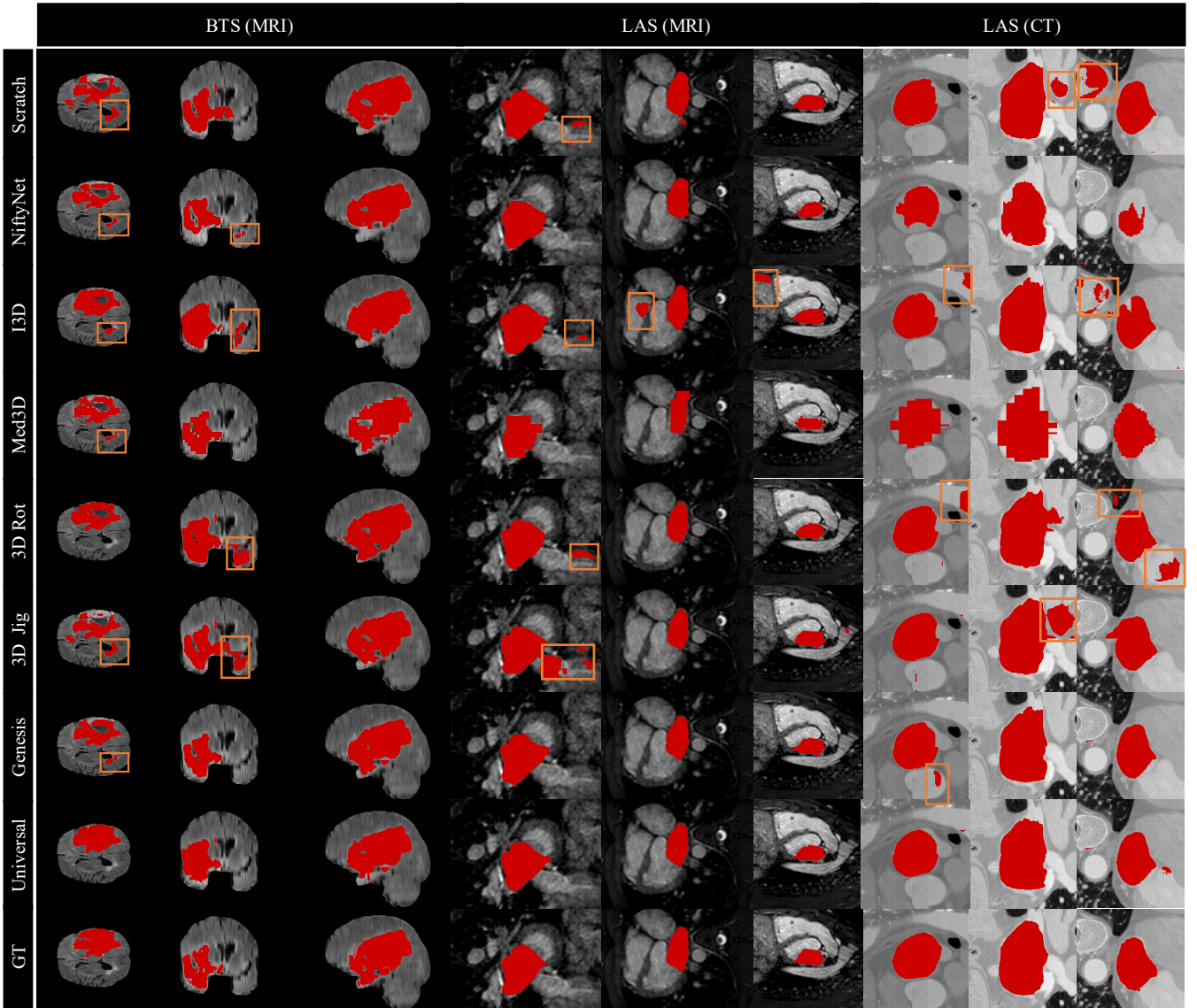


Fig. 3. Representative results for three target segmentation tasks produced by different methods, where GT presents the ground truth. The results are shown as multi-view image slices sampled on axial, coronal, and sagittal. The orange boxes indicate where the models segment incorrectly.

B. Analytical ablation studies

1) *Necessity of Multi-Modal Data*: We conduct ablation experiments to analyze the performance gap caused by the modality discrepancy between the target dataset and the dataset

used in model pre-training. We thus apply the basic self-supervised learning framework on different combinations of multi-modality datasets, including CT only ($Model_{CT}$), MRI only ($Model_{MRI}$) and both ($Model_{Multi}$). To some extent,

TABLE IV

ABLATION STUDY RESULTS FOR THE FIVE TARGET TASKS. $Model_{CT}$, $Model_{MRI}$, $Model_{Multi}$ CORRESPOND TO THE PRE-TRAINED MODELS WITH CT ONLY, MRI ONLY AND ALL OF THE DATASETS, RESPECTIVELY. $Model_{Multi+MIAL}$ AND $Model_{Multi+SC}$ REPRESENT ADDING THE PROPOSED MIAL MODULE AND THE SCALE CLASSIFIER TO $Model_{Multi}$, RESPECTIVELY.

Pre-training Approach	Used to Pre-train Universal Model		Not Used to Pre-train Universal Model		
	BTS (MRI) IoU (%)	LNC(CT) AUC (%)	LAS (CT) IoU (%)	LAS (MRI) IoU (%)	ADC (MRI) AUC (%)
Train from scratch	58.52 \pm 2.61	94.25 \pm 5.07	68.29 \pm 1.68	67.04 \pm 2.18	74.00 \pm 3.82
Model Genesis	67.96 \pm 1.29	98.34 \pm 0.44	76.48 \pm 2.89	74.53 \pm 1.69	79.33 \pm 2.29
$Model_{CT}$	67.76 \pm 0.93	98.77 \pm 0.26	76.52 \pm 2.09	74.81 \pm 1.12	79.11 \pm 3.12
$Model_{MRI}$	68.19 \pm 0.89	97.08 \pm 0.25	69.23 \pm 1.55	74.98 \pm 0.72	80.13 \pm 2.36
$Model_{Multi}$	69.85 \pm 0.79	98.90 \pm 0.10	76.94 \pm 2.80	75.33 \pm 0.87	82.22 \pm 3.37
$Model_{Multi+MIAL}$	70.76 \pm 0.58	99.31 \pm 0.27	77.19 \pm 1.05	76.13 \pm 0.44	82.44 \pm 3.54
$Model_{Multi+SC}$	71.14 \pm 0.61	98.94 \pm 0.25	75.83 \pm 0.49	75.62 \pm 0.33	83.00 \pm 3.40
Universal Model (Ours)	72.10 \pm 0.67	99.04 \pm 0.23	78.14 \pm 0.77	77.52 \pm 0.50	86.44 \pm 1.09

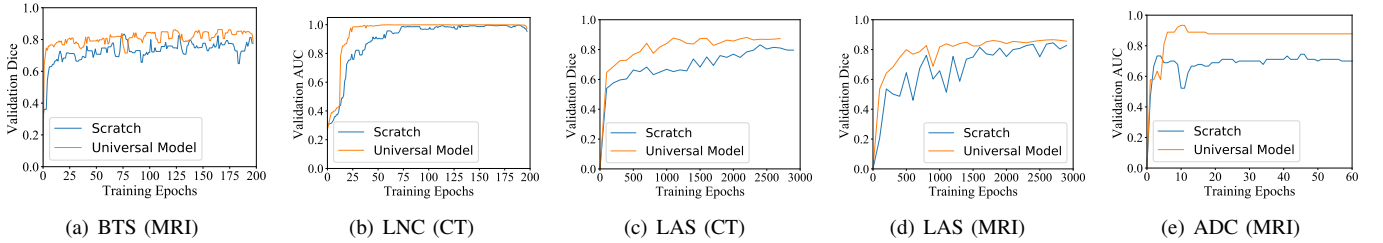


Fig. 4. Comparison of the validation curves for five target tasks, in which Dice scores and AUC scores are reported for segmentation and classification tasks, respectively.

$Model_{Multi}$ is a naive extension of Model Genesis on multiple datasets, showing better performance. As shown in Table IV, the performance of same-modality transfer learning is always better since relatively small discrepancies make the learned representation more favorable. It is also observed that the $Model_{Multi}$ increases the overall performance by 2.09 (67.76% vs 69.85%), 0.52 (74.81% vs 75.33%), 3.11 (79.11% vs 82.22%) on the three MRI tasks compared with $Model_{CT}$ and 1.82 (97.08% vs 98.90%), (7.71 (69.23% vs 76.94%) on the two CT tasks compared with $Model_{MRI}$. This result suggests the intuitive reason that aggregating multi-modality data for network training gains more information and demonstrates the necessity of using multi-modality data for general representation learning.

2) Effectiveness of Proposed Modules: Instead of using solely self-supervised learning framework and jointly learning from simply mixing the multi-modal datasets, Universal Model adopts two modules to further learning multi-level modality invariant representations. We further validate the effectiveness of the proposed two key modules. $Model_{Multi+MIAL}$ and $Model_{Multi+SC}$ represent the basic model combined with corresponding module trained with multiple datasets. As can be seen, the proposed MIAL module achieves a significant gain over $Model_{Multi}$ for all the five tasks, with 0.91%, 0.41%, 0.25%, 0.80%, 0.22% gains on IoU/AUC scores, respectively. This indicates that MIAL module successfully benefits the generalizable and robust representation learning for multi-modal medical data, which also meets our hypothesis on modality-invariant feature learning. Besides, incorporating our proposed SC module significantly improves the segmentation performance over $Model_{Multi}$ (e.g. 1.29% for BTS (MRI) and 0.29% for LAS (MRI)). As described in Section III-

C, multi-scale were integrated into our pre-trained model to learn comprehensive contextual and hierarchically geometric features at different levels. Based on the above ablation studies, we can conclude that the adoption of the two modules yields much better results than simply extending Model Genesis on multiple datasets ($Model_{Multi}$). It is worthy to point out that our proposed pre-trained model not only has higher performance but also shows stronger robustness and less fluctuation of results.

C. Analysis of Convergence Speed

We compare the convergence speed of the proposed pre-trained model and training from scratch. A good weight initialization can prevent layer activation outputs from exploding or vanishing during the course of a back propagation through a deep neural network. As shown in Fig. 4, Universal Model converges fast to a stable loss and achieves a high validation dice coefficient. Correspondingly, models trained from scratch have much higher fluctuation and much slower convergence. This suggests that the proposed representation learning scheme for the Universal Model can speed up the convergence and boost the performance compared to training from scratch. Meanwhile, we observe that the pre-trained model provides a better starting point for the network, leading to a higher starting validation score for five target tasks consistently.

D. Analysis of Annotation Cost

The performance of computer vision tasks increases logarithmically with the amount of training data [49]. To validate the gains in data-efficiency, we train the model with different proportions (10%, 30%, 70%, 100%) of the training data and

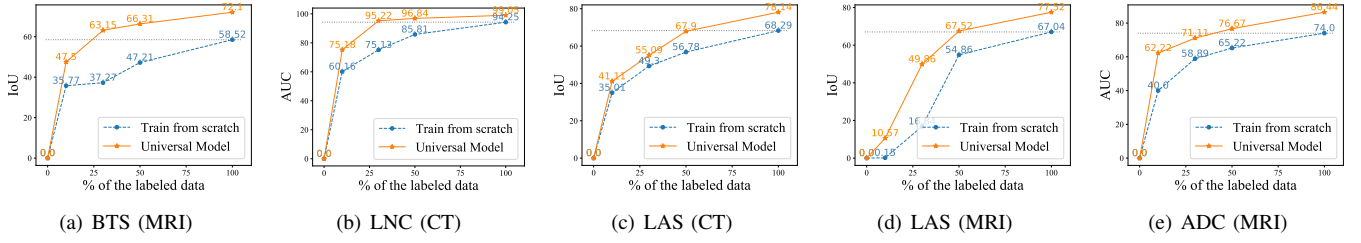


Fig. 5. Comparison of experiment results for five target tasks at different ratios of annotated data. The gray dash lines refer to the performance of training from scratch with the entire dataset.

TABLE V

EXPERIMENT RESULTS WITH LABEL CORRUPTION FOR THREE SEGMENTATION TARGET TASKS. THE MEAN AND STANDARD DEVIATION OF IOU SCORES(%) ARE REPORTED ACROSS FIVE TRIALS.

Target Task	Random	Model Genesis	Universal Model
BTS (MRI)	52.79 \pm 5.28	67.45 \pm 1.51	70.86 \pm 0.76
LAS (CT)	62.09 \pm 2.73	68.49 \pm 3.44	71.06 \pm 1.53
LAS (MRI)	64.36 \pm 0.60	72.36 \pm 1.26	73.61 \pm 1.08

use the same test set to measure the performance. Fig. 5 displays the results compared with training from scratch. The model performance drops sharply when decreasing the training data due to the overfitting issue. Not surprisingly, fine-tuning on top of our pre-trained model can significantly improve performance on all data sizes. The pre-trained model leads to a reduction on the annotation cost by at least 50% on the target tasks compared with training from scratch.

E. Robustness Analysis of Noisy Labels

High-quality expert annotation in medical imaging data is the key factor to obtain high performance in deep learning. However, the quality of annotations relies heavily on the experience of labeling radiologists. In this section, we evaluate Universal Model on the three segmentation target tasks with simulated noisy masks and show that pre-training does markedly improve model robustness. We randomly erode and dilate the masks to imitate the errors in the annotation process. As shown in Table V, Universal Model achieves a significant gain over random initialization for all the three tasks of 18.07%, 8.97%, 9.25% on IoU score. More importantly, the performance obtained by our approach is higher than Model Genesis for all the three tasks of 3.41%, 2.57%, 1.25%, which shows that Universal Model is more robust.

VI. CONCLUSION AND DISCUSSION

In this paper, we aim to build a generalizable pre-trained model that can be effectively adopted by a variety of 3D medical image analysis tasks in multiple modalities. This problem has not been well studied for 3D medical images so far, compared with its correspondence in the natural image domain, mainly due to limited annotations for medical images and significant distribution discrepancy across modalities. Model Genesis [14] is the recent state-of-the-art on this topic, which learns directly from unlabeled 3D image data via self-supervision. However, it is not targeted for the multi-modality

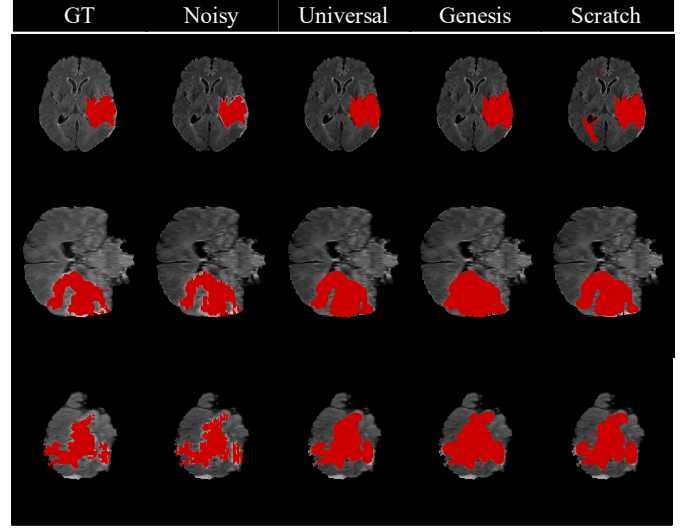


Fig. 6. Representative example of the results on BTS (MRI) with noisy masks as training label, where GT presents the ground truth, Noisy shows the generated noisy masks. We show the 3D results by multi-view image slices sampled on axial, coronal, sagittal.

and multi-task generalization. To handle the multi-modality and multi-task generalization problem for 3D medical image analysis, we here propose an effective and universal pre-trained model, which involves a modality invariant adversarial learning module for modality invariant representations and a scale classifier to recognize multi-scale sub-volume inputs so as to capture multi-level contextual features. We verify the generalization of Universal Model comprehensively on five distinctive target tasks. The experimental results have demonstrated that our pre-trained model significantly improves the performance of the common training from scratch strategy and also outperforms the state-of-the-art transfer learning methods for 3D medical images. We believe our work provides new insights into universal model pre-training and serves as a milestone in 3D medical image analysis.

The employed 3D U-Net are relatively basic but widely used, compared with a more complicated network for specific target tasks. This is reasonable as we currently focus on proposing a general and transferable pre-training model. However, the encoder may not be the most suitable feature extractor for all target tasks due to its plain architecture. Therefore, as our future work, we plan to integrate our MIAL module and SC module into well-designed networks, seeking a more comprehensive application in medical image analysis.

REFERENCES

- [1] H.-C. Shin *et al.*, “Deep convolutional neural networks for computer-aided detection: Cnn architectures, dataset characteristics and transfer learning,” *IEEE Transactions on Medical Imaging*, vol. 35, no. 5, pp. 1285–1298, 2016.
- [2] J. Deng, W. Dong, R. Socher, L. Li, Kai Li, and Li Fei-Fei, “Imagenet: A large-scale hierarchical image database,” in *IEEE Conference on Computer Vision and Pattern Recognition*, pp. 248–255, 2009.
- [3] N. Tajbakhsh *et al.*, “Convolutional neural networks for medical image analysis: Full training or fine tuning?,” *IEEE Transactions on Medical Imaging*, vol. 35, no. 5, pp. 1299–1312, 2016.
- [4] Z. Guodong and Z. Guoyan, “Deep learning-based automatic segmentation of the proximal femur from mr images,” in *Intelligent Orthopaedics: Artificial Intelligence and Smart Image-guided Technology for Orthopaedics*, pp. 73–79, 2018.
- [5] Y. Xin, B. Cheng, Y. Lequan, N. Dong, and H. Pheng-Ann, “Hybrid loss guided convolutional networks for whole heart parsing,” in *Statistical Atlases and Computational Models of the Heart. ACDC and MMWHS Challenges*, pp. 215–223, 2018.
- [6] J. Carreira and A. Zisserman, “Quo vadis, action recognition? a new model and the kinetics dataset,” in *IEEE Conference on Computer Vision and Pattern Recognition*, pp. 4724–4733, 2017.
- [7] D. Tran, L. Bourdev, R. Fergus, L. Torresani, and M. Paluri, “C3d: Generic features for video analysis,” *arXiv preprint arXiv:1412.0767*, 2014.
- [8] Q. Liu, Q. Dou, L. Yu, and P. A. Heng, “Ms-net: Multi-site network for improving prostate segmentation with heterogeneous mri data,” *IEEE Transactions on Medical Imaging*, vol. 39, no. 9, pp. 2713–2724, 2020.
- [9] S. Chen, K. Ma, and Y. Zheng, “Med3d: Transfer learning for 3d medical image analysis,” *arXiv preprint arXiv:1904.0062*, 2019.
- [10] Z. Zongwei *et al.*, “Models genesis: Generic autodidactic models for 3d medical image analysis,” in *Medical Image Computing and Computer Assisted Intervention*, pp. 384–393, 2019.
- [11] L. Chen, P. Bentley, K. Mori, K. Misawa, M. Fujiwara, and D. Rueckert, “Self-supervised learning for medical image analysis using image context restoration,” *Medical Image Analysis*, vol. 58, p. 101539, 2019.
- [12] X. Zhuang, Y. Li, Y. Hu, K. Ma, Y. Yang, and Y. Zheng, “Self-supervised feature learning for 3d medical images by playing a rubik’s cube,” in *Medical Image Computing and Computer Assisted Intervention*, pp. 420–428, 2019.
- [13] A. Taleb *et al.*, “3d self-supervised methods for medical imaging,” *arXiv preprint arXiv:2006.03829*, 2020.
- [14] Z. Zhou, V. Sodha, J. Pang, M. B. Gotway, and J. Liang, “Models genesis,” *arXiv preprint arXiv:2004.07882*, 2020.
- [15] G. J. S. Litjens *et al.*, “A survey on deep learning in medical image analysis,” *Medical Image Analysis*, vol. 42, pp. 60–88, 2017.
- [16] H. Greenspan, B. van Ginneken, and R. M. Summers, “Guest editorial deep learning in medical imaging: Overview and future promise of an exciting new technique,” *IEEE Transactions on Medical Imaging*, vol. 35, pp. 1153–1159, 2016.
- [17] Z. Zhou *et al.*, “Fine-tuning convolutional neural networks for biomedical image analysis: Actively and incrementally,” in *IEEE Conference on Computer Vision and Pattern Recognition*, pp. 4761–4772, 2017.
- [18] L. Lu, Y. Zheng, G. Carneiro, and L. Yang, *Deep Learning and Convolutional Neural Networks for Medical Image Computing: Precision Medicine, High Performance and Large-Scale Datasets*. Advances in Computer Vision and Pattern Recognition, 2017.
- [19] A. Esteva *et al.*, “Dermatologist-level classification of skin cancer with deep neural networks,” *Nature*, vol. 542, pp. 115–118, 2017.
- [20] C. Szegedy, V. Vanhoucke, S. Ioffe, J. Shlens, and Z. Wojna, “Rethinking the inception architecture for computer vision,” in *IEEE Conference on Computer Vision and Pattern Recognition*, pp. 2818–2826, 2016.
- [21] N. Tajbakhsh, J. Y. Shin, M. B. Gotway, and J. Liang, “Computer-aided detection and visualization of pulmonary embolism using a novel, compact, and discriminative image representation,” *Medical Image Analysis*, vol. 58, p. 101541, 2019.
- [22] A. Taleb, C. Lippert, T. Klein, and M. Nabi, “Multimodal self-supervised learning for medical image analysis,” *arXiv preprint arXiv:1912.05396*, 2019.
- [23] A. Taleb, W. Löttsch, N. Danz, J. Severin, T. Gärtner, and B. Bergner, “3d self-supervised methods for medical imaging,” *arXiv preprint arXiv:2006.03829*, 2020.
- [24] F. Haghighi, M. R. H. Taher, Z. Zhou, M. B. Gotway, and J. Liang, “Learning semantics-enriched representation via self-discovery, self-classification, and self-restoration,” *arXiv preprint arXiv:2007.06959*, 2020.
- [25] Y. Ganin and V. S. Lempitsky, “Unsupervised domain adaptation by backpropagation,” in *International Conference on Machine Learning*, 2015.
- [26] E. Tzeng, J. Hoffman, K. Saenko, and T. Darrell, “Adversarial discriminative domain adaptation,” in *IEEE Conference on Computer Vision and Pattern Recognition*, pp. 2962–2971, 2017.
- [27] Z. Pei, Z. Cao, M. Long, and J. Wang, “Multi-adversarial domain adaptation,” in *AAAI*, 2018.
- [28] Y. Zhang, Y. Zhang, Y. Wang, and Q. Tian, “Domain-invariant adversarial learning for unsupervised domain adaption,” *arXiv preprint arXiv:1811.12751*, 2018.
- [29] I. J. Goodfellow *et al.*, “Generative adversarial networks,” *arXiv preprint arXiv:1406.2661*, 2014.
- [30] H. Li, S. J. Pan, S. Wang, and A. C. Kot, “Domain generalization with adversarial feature learning,” in *IEEE Conference on Computer Vision and Pattern Recognition*, pp. 5400–5409, 2018.
- [31] Q. Dou, C. Ouyang, C. Chen, H. Chen, and P.-A. Heng, “Unsupervised cross-modality domain adaptation of convnets for biomedical image segmentations with adversarial loss,” *IJCAI*, 2018.
- [32] C. Ouyang, K. Kamnitsas, C. Biffi, J. Duan, and D. Rueckert, “Data efficient unsupervised domain adaptation for cross-modality image segmentation,” in *Medical Image Computing and Computer Assisted Intervention*, pp. 669–677, 2019.
- [33] Ö. Çiçek, A. Abdulkadir, S. S. Lienkamp, T. Brox, and O. Ronneberger, “3d u-net: Learning dense volumetric segmentation from sparse annotation,” in *Medical Image Computing and Computer Assisted Intervention*, pp. 424–432, 2016.
- [34] D. Pathak, P. Krähenbühl, J. Donahue, T. Darrell, and A. A. Efros, “Context encoders: Feature learning by inpainting,” in *IEEE Conference on Computer Vision and Pattern Recognition*, pp. 2536–2544, 2016.
- [35] F. Isensee *et al.*, “nnu-net: Self-adapting framework for u-net-based medical image segmentation,” *arXiv preprint arXiv:1809.10486*, 2018.
- [36] A. A. A. Setio, C. Jacobs, J. Gelderblom, and B. van Ginneken, “Automatic detection of large pulmonary solid nodules in thoracic ct images,” *Medical physics*, vol. 42, pp. 5642–5653, 2015.
- [37] P. Bilic *et al.*, “The liver tumor segmentation benchmark (lits),” *arXiv preprint arXiv:1901.04056*, 2019.
- [38] B. H. Menze *et al.*, “The multimodal brain tumor image segmentation benchmark (brats),” *IEEE Transactions on Medical Imaging*, vol. 34, no. 10, pp. 1993–2024, 2015.
- [39] S. Bakas *et al.*, “Identifying the best machine learning algorithms for brain tumor segmentation, progression assessment, and overall survival prediction in the brats challenge,” *arXiv preprint arXiv:1811.02629*, 2018.
- [40] A. L. Simpson *et al.*, “A large annotated medical image dataset for the development and evaluation of segmentation algorithms,” *arXiv preprint arXiv:1902.09063*, 2019.
- [41] X. Zhuang, “Challenges and methodologies of fully automatic whole heart segmentation: a review,” *Journal of healthcare engineering*, vol. 43, pp. 371–408, 2013.
- [42] X. Zhuang and J. Shen, “Multi-scale patch and multi-modality atlases for whole heart segmentation of mri,” *Medical Image Analysis*, vol. 31, pp. 77 – 87, 2016.
- [43] S. G. Mueller *et al.*, “The alzheimer’s disease neuroimaging initiative,” *Neuroimaging Clinics*, vol. 15, no. 4, pp. 869–877, 2005.
- [44] C. Yang, A. Rangarajan, and S. Ranka, “Visual explanations from deep 3d convolutional neural networks for alzheimer’s disease classification,” *American Medical Informatics Association Annual Symposium*, vol. 2018, pp. 1571–1580, 2018.
- [45] D. Kingma and J. Ba, “Adam: A method for stochastic optimization,” in *International Conference on Learning Representations*, vol. 42, 2014.
- [46] E. Gibson *et al.*, “Niftynet: a deep-learning platform for medical imaging,” *Computer Methods and Programs in Biomedicine*, vol. 158, pp. 113 – 122, 2018.
- [47] W. Kay *et al.*, “The kinetics human action video dataset,” *arXiv preprint arXiv:1705.06950*, 2017.
- [48] E. Gibson *et al.*, “Automatic multi-organ segmentation on abdominal ct with dense v-networks,” *IEEE Transactions on Medical Imaging*, vol. 37, pp. 1822–1834, 2018.
- [49] C. Sun, A. Shrivastava, S. Singh, and A. Gupta, “Revisiting unreasonable effectiveness of data in deep learning era,” in *IEEE International Conference on Computer Vision*, pp. 843–852, 2017.